

# Evaluation of a photon-counting breast tomosynthesis imaging system

Andrew D.A. Maidment<sup>a\*</sup>, Christer Ullberg<sup>b</sup>, Karin Lindman<sup>b</sup>, Leif Adelöw<sup>b</sup>,  
Johan Egerström<sup>b</sup>, Mathias Eklund<sup>b</sup>, Tom Francke<sup>b</sup>, Ulf Jordung<sup>b</sup>, Tomas Kristoffersson<sup>b</sup>,  
Lars Lindqvist<sup>b</sup>, Daniel Marchal<sup>b</sup>, Hans Olla<sup>b</sup>, Erik Penton<sup>b</sup>, Juha Rantanen<sup>b</sup>,  
Skiff Solokov<sup>b</sup>, Niclas Weber<sup>b</sup>, Hans Westerberg<sup>b</sup>

a) University of Pennsylvania, Philadelphia PA, USA

b) XCounter AB, Svärdvägen 11, SE-182 33 Danderyd, Sweden

## ABSTRACT

Digital breast tomosynthesis promises solutions to many of the problems associated with projection mammography, including elimination of artifactual densities due to the superposition of normal tissues and increasing the conspicuity of true lesions that would otherwise be masked by superimposed normal tissue. We have investigated tomosynthesis using a digital camera containing 48 photon counting, orientation sensitive, linear detectors which are precisely aligned with the focal spot of the x-ray source. The x-ray source and the digital detectors are scanned in a continuous motion across the object (patient), each linear detector collecting an image at a distinct angle. A preliminary assessment of tomosynthesis image quality has been performed with both qualitative and quantitative methods. Measured values of MTF and NPS appear concordant with theoretical values. The MTF in the scanning direction is dominated by scanning unsharpness and geometric factors, while the NPS is white. The MTF and NPS in the strip direction are somewhat lower than in the scan direction. The NPS of tomographic images show a slight decrease with increasing spatial frequency, related to the sampling and interpolation in the reconstruction process. A phase I clinical trial is ongoing; 9 women have been recruited. Breast positioning is comparable to other imaging systems. The visualization of breast anatomy appears to be superior to screen-film mammography, at the same average glandular dose. Examination of images reconstructed with a sub-sampled set of projection images appears to support the hypothesis that image quality is superior when more projection images are used in the reconstruction.

**Keywords:** Digital breast tomosynthesis, synthetic tomography, digital mammography, modulation transfer function (MTF), noise power spectra (NPS), clinical trial.

## 1. INTRODUCTION

There are two key problems currently associated with projection mammography.<sup>1</sup> First, artifactual densities can arise from the superposition of normal tissues; such densities can result in a loss of specificity. Second, true lesions often lack conspicuity or are morphologically ill-defined as they are masked by superimposed normal tissue, potentially reducing both sensitivity and specificity. Tomosynthesis is a promising solution to overcome these problems, providing tomographic images of the breast while also providing a simple means of localizing lesions in three-dimensions.<sup>2-7</sup>

A novel tomosynthesis system (XC Mammo-3T, XCounter AB, Danderyd, Sweden) has been developed for mammography screening and diagnosis. The system differs fundamentally from other breast tomosynthesis systems in that it simultaneously acquires a large number of images free of electronic noise and scattered x-rays, using a novel scanning method. Current competing tomosynthesis implementations use a mammographic area detector to repeatedly acquire images in which the projection angle is slowly altered either continuously or discretely. Such designs naturally suffer problems which can potentially degrade tomographic image quality. Specifically, the requirement of repeated exposures from an individual detector requires a trade-off between scan time and the number of acquisition angles. As demonstrated previously, image artifacts are better suppressed when more projection images are used to produce the tomographic reconstructions.<sup>7</sup> In addition, current area detectors are energy-integrating, and thus suffer from various sources of electronic noise, as well as ghosting and lag.<sup>8</sup> These imperfections in the detector serve to further degrade the resulting tomographic image quality.

\* [Andrew.Maidment@uphs.upenn.edu](mailto:Andrew.Maidment@uphs.upenn.edu); Phone +1 215 746-8763; Fax +1 215 746-8764

Digital breast tomosynthesis is a new and developing field; the results presented here are part of an ongoing work-in-progress. We have sought to both qualitatively and quantitatively assess system technical and clinical performance, and to optimize system design. In this paper, we report preliminary measures of imaging performance and a phase I clinical trial. Continuing the research presented last year, we again examine the role of the number of projection angles on the image quality of the reconstructed tomosynthesis images.

## 2. METHODS AND MATERIALS

### 2.1. System Design

The imaging system uses 48 photon counting, orientation sensitive, linear detectors which are precisely aligned with the focal spot of the x-ray source. The x-ray source and the digital detectors are scanned in a continuous motion across the object (patient); each linear detector collecting an image at a distinct angle. The 48 simultaneously collected images are of a very high image quality due to several special characteristics of this detector technology. First, the detectors are insensitive to scattered radiation; the detector geometry ensures that essentially only primary photons emanating from the focal spot of the x-ray source will elicit a response from the detector. Second, the detector does not contribute any electronic noise; the strong gaseous amplification of each x-ray interaction allows a simple threshold to exclude electronic noise from being counted and included in the final image. Third, each line of the image is rapidly acquired (typically  $<2$  ms), minimizing any motion blurring. Fourth, the large number of images acquired simultaneously significantly reduces the reconstruction artifacts in the reconstructed planes.<sup>7</sup> Finally, the detector technology is free of lag avoiding ghosting artifacts, and has very high dynamic range thus avoiding blooming.

The system consists of an E-arm that is scanned across the breast, as shown in Figure 1. The E-arm supports the x-ray tube, pre-patient collimator and camera. The x-ray source is a tungsten-anode mammography tube (Varian, RAD 70T). The x-ray flux is filtered through a 0.5 mm aluminum filter. The x-ray field is split into 48 fan-shaped beams by a tungsten pre-patient collimator positioned just above the breast. The camera, consisting of 48 sensor rows enclosed in a steel gas-tight box, moves under the breast. The camera box is filled with a noble gas at a few atmospheres pressure. The linear sensors occupy an active area of  $24 \times 30$  cm<sup>2</sup>. The pixel size is 60  $\mu$ m and each sensor is read out every 60  $\mu$ m during the scan.

Three dimensional tomographic images are reconstructed using a filtered back-projection method, in slices parallel with the detector spaced every 1 mm. Both the tomographic and source images are displayed using custom software. The software presents the images in stack mode. The reader can magnify, pan, and window and level the images.

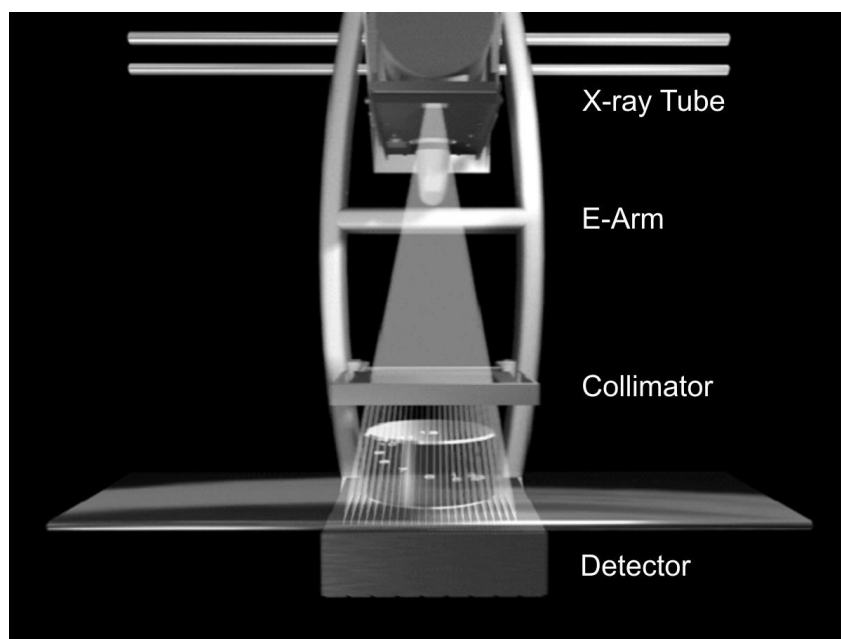


**Figure 1:** Schematic of the imaging system. The system consists of an E-arm, on which are mounted the x-ray tube, collimator and detector. The collimator is used to define 48 linear x-ray beams which are precisely aligned with the x-ray tube and detector. Images are produced by linearly scanning the E-arm past the breast; in the process, 48 images of the breast are produced, each at a unique angle.

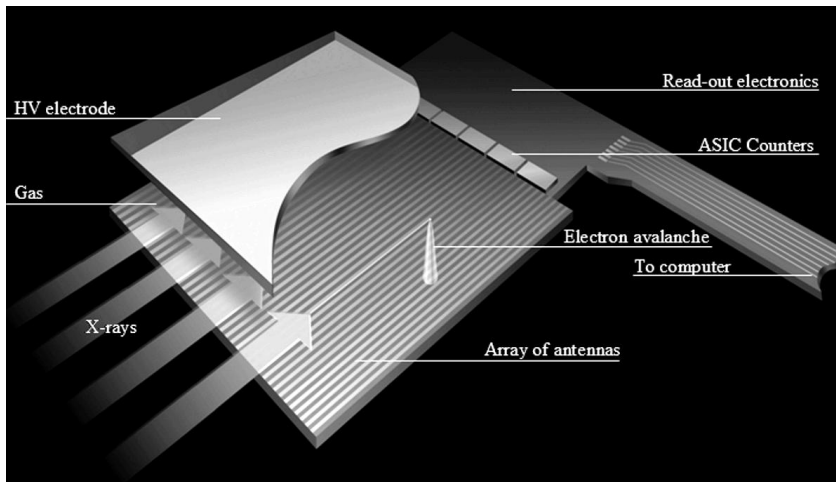


**Figure 2:** Schematic of a detector array. The detector array consists of two parallel electrodes. X rays enter parallel to the electrodes, and interact with a noble gas. An electric potential is applied to the electrodes. The detector design is such that an avalanche of electrons is triggered. If the shaped pulse exceeds a specific threshold, then a counter for that detector element within the ASIC is incremented.

The individual gaseous avalanche x-ray sensors operate on the principle of photon counting. The x rays interact in the gas and liberate charges producing an image of the x-ray flux transmitted through the patient. The detector is shown in schematic in Figure 2. The detector consists of 2 electrodes: one continuous; the other forming pixels aligned with the divergent x-ray beam. The x rays enter one-by-one into the gas between the electrodes and ionize the gas, liberating electrons. A voltage applied between the electrodes causes these electrons to move towards the positive anode. These electrons further ionize the gas, knocking out new electrons and triggering an avalanche of electrons. Hence, the energy from each x ray is amplified many-fold. The gain of the gaseous avalanche is such that only x rays (or gamma rays) are sufficient to produce an avalanche, and a simple threshold can be used to discriminate the x rays. As a result, there is no dark current, and the image noise is limited by the Poisson statistical fluctuation of the incoming x-ray flux.

As discussed previously,<sup>5-7</sup> the system is insensitive to scattered x rays; only x rays traveling in a straight line from the focal spot of the x-ray source can enter between the electrodes and liberate sufficient charge to trigger an avalanche.

The system is typically operated between 30 and 40 kVp, at up to 210 mA. The kVp, mA and integration time (scan speed) can be altered to achieve a specific breast or detector dose. Forty-eight source images appropriate for tomosynthesis reconstruction can be acquired over a region of 24×30 cm<sup>2</sup> within 10-20 seconds. Optimization as a function of breast size and thickness is ongoing. The techniques used in the current clinical trial are designed to use an average glandular dose (AGD) less than or equal to screen-film mammography. It is our belief that the absence of electronic noise and scatter facilitate this choice. As discussed in Section 3.2, it appears that this choice results in clinically acceptable image quality.

## 2.2. MTF and NPS Measurement Techniques

The pre-sampled modulation transfer function (MTF) was measured using the slanted edge method.<sup>9-11</sup> The edge was made of 50 μm thick tungsten foil and was placed directly on the breast support at an angle of approximately 1.5°. A technique of 35 kVp was used. An additional 40 mm of PMMA was placed directly above the edge to appropriately harden the beam. This geometry is consistent with clinical practice, and thus the measurements reflect the “system MTF”; namely, the MTF of the system including all possible sources of image blurring and degradation, such as scatter.<sup>10, 12</sup> In the data presented, the tomosynthesis plane with the edge in focus was reconstructed using backprojection without a frequency-dependent filter.

The noise power spectra (NPS) were measured using the same spectrum (applied voltage and filtration) as for the MTF measurement, with a dose corresponding to an AGD of 1.5 mGy for a 40 mm breast. Ten planes nearest the bottom edge of the 40 mm PMMA phantom (vertically) were reconstructed with 1 mm spacing using backprojection without a frequency-dependent filter. A 1024×2048 pixel region of interest (ROI) close to the chestwall was selected. The 2D NPS was then calculated from 256×256 pixel ROI overlapped by 128 pixels in each direction, by averaged over all sub regions and all reconstructed planes. The 1D NPS were then extracted from the 2D spectra. Using the method of Bendat and Piersol,<sup>13</sup> we calculate that the standard error in the NPS estimates is 3.2%

### 2.3. Clinical Trial Design

A phase I clinical trial involving 30 women is ongoing. The trial is being conducted jointly at Danderyds Sjukhus AB (Danderyds, Sweden) and XCounter AB. At the time of the conference (Feb. 10, 2006), 9 women had participated in the imaging trial. Participants of the trials must be at least 40 years of age, and pregnant women are excluded from the trial. All diagnostic patients at Danderyds Sjukhus are eligible; these specifically include women recalled from screening, and women referred for clinical reasons. Screen-film mammography is performed at the Danderyds Sjukhus Mammography Department per clinical practice. Images are acquired on one of two mammography systems: a Siemens Mammomat 3000 (Siemens, Erlangen, Germany) or a Planmed Sophie (Planmed Oy, Helsinki, Finland). Both systems have a molybdenum target and filter. Films are typically acquired at 30-31 kVp, and are phototimed.

The tomosynthesis images are acquired at XCounter on the same day by the same radiologic nurse. Only one breast is imaged in a single view. Due to initial mechanical constraints, the first 6 patients were imaged in a CC orientation. The most recent three patients were imaged in an MLO orientation. Currently, all patients have been imaged at 35 kVp, 140-180 mA with a 2 ms integration time, resulting in a scan time of 17 seconds. Note that any one part of the breast is only in the x-ray beam for 10 seconds, thus minimizing the risk of motion unsharpness. This technique was chosen to result in an AGD of approximately 1.5 mGy. Tomosynthesis images are being reviewed prospectively by Dr. Per Sunden (Danderyds Sjukhus AB). A retrospective trial of image quality is planned, but is beyond the scope of this paper.

## 3. RESULTS AND DISCUSSION

### 3.1. System Performance

The MTF in the scanning and strip (i.e., parallel to the linear detector strips) directions have been measured. Figure 3 shows the measured MTF in the scanning direction. These data are shown compared to theoretical calculations. The theoretical MTF can be decomposed into 2 main sources of blurring. The first is related to scanning unsharpness. The detector is read out each time the detector array is translated  $60\ \mu\text{m}$ . Thus, the scanning unsharpness can be represented by an appropriate sinc function. The second source of unsharpness is related to the image acquisition geometry; the collimator is at a fixed distance above the breast and the x-ray focal spot is of known size and shape. Thus, it is possible to calculate the blurring due to the collimator width and geometric unsharpness as the product of two sinc functions, assuming that the focal spot has a rectangular intensity profile. The product of these two sources of unsharpness is specified as the "Total" in Figure 3. The similarity of the measured and experimental data is noteworthy. The discrepancy seen is likely due to deviation from the assumption of a rectangular focal spot.

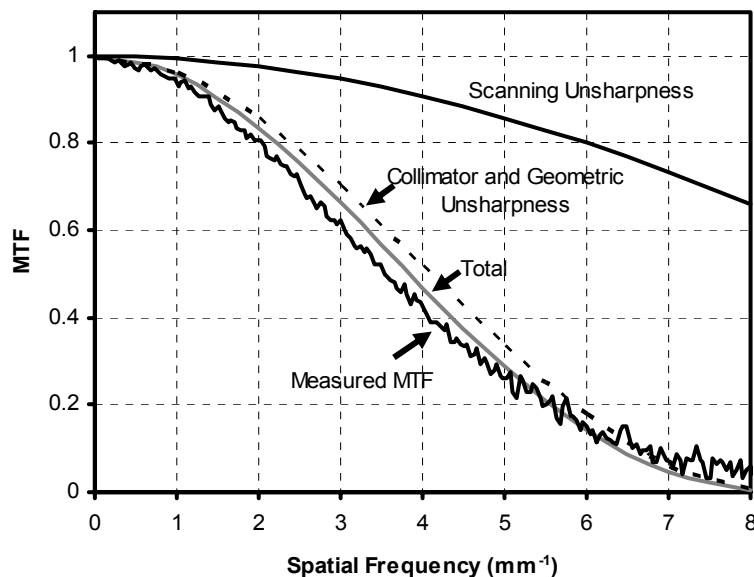


**Figure 3:** System MTF of tomographic images in the scanning direction. Both measured and theoretical data are presented. The theoretical unsharpness is divided into two terms: scanning unsharpness, and collimator and geometric unsharpness. Their product is labeled "Total". The theoretical total MTF is quite similar to the measured MTF.

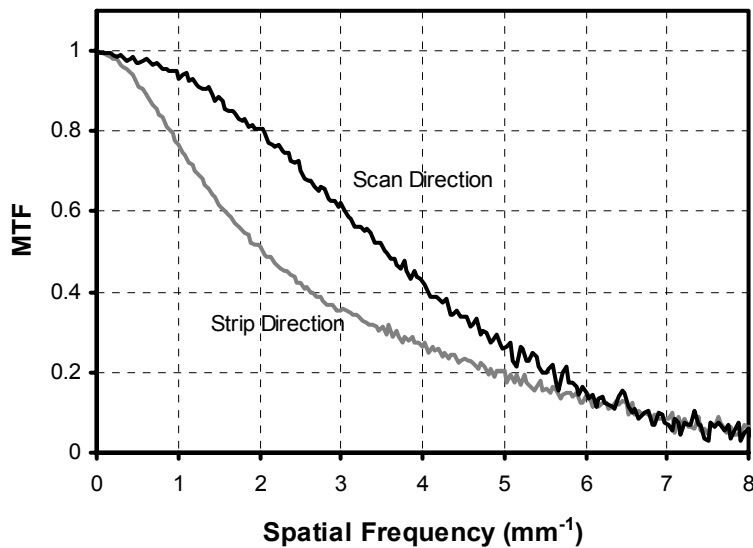


**Figure 4:** MTF of tomographic images in the scan and strip directions. The MTF in the strip direction is reduced compared to the scan direction due to simultaneous triggering of adjacent channels.

Figure 4 shows the measured MTF in the scan and strip directions. The resolution in the strip direction is lower than that in the scan direction. This degradation is still under investigation; however, it is likely due to simultaneous triggering of adjacent channels.

The measured NPS are shown in Figure 5. The NPS have been normalized to unity at their maximum, except the NPS for the projection images in the scanning direction (solid squares) were normalized by their mean. The NPS in the scanning direction are shown as solid symbols, while the NPS in the strip direction are shown as open symbols. The NPS of the projection images ( $NPS_P$ ) are shown as rectangles. The NPS in the scanning direction (solid squares) is white. This is expected, as each line is acquired independently (sequentially in time), and the system is free of lag; thus, there should be no correlation between neighboring lines in the image. By comparison, the NPS in the strip direction (open squares) shows some correlation, which manifests itself as a reduction at high frequencies. It is likely that the correlation seen in the NPS is due to the same phenomenon responsible for a reduction in the MTF in the strip direction.

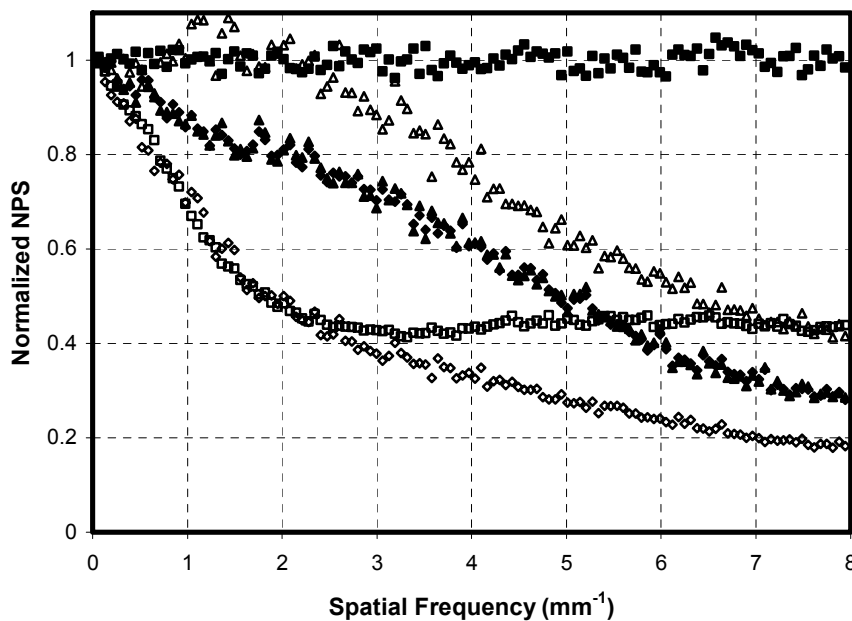


**Figure 5:** NPS measurements in the scan (solid symbols) and strip (open symbols) directions. The  $NPS_P$  of the source (projection) images are given by squares, while the  $NPS_T$  of the tomographic (reconstructed) images are given by diamonds. The ratio of  $NPS_T/NPS_P$  are given by triangles. Note that in the scanning direction  $NPS_T$  and  $NPS_T/NPS_P$  are difficult to distinguish because  $NPS_P$  is white.

The NPS of the reconstructed tomographic images ( $NPS_T$ ) are shown as diamonds. The  $NPS_T$  is reduced in both the scanning and strip directions. To understand the source of this correlation, we took the ratio of the  $NPS_T/NPS_P$ . As expected, the ratio in the scanning direction (solid triangles) is indistinguishable from  $NPS_T$  in that direction. The ratio in the strip direction (open triangles) has a similar shape to that in the scanning direction. We believe that both sources of correlation have the same origins; namely, the correlation arises from interpolation of the projection data in the back-projection operation. We are currently investigating this further.

It should be noted that both the NPS and the MTF were measured with a 40 mm PMMA phantom in the same position as the breast. As a result, the presented data should be interpreted as the “system MTF” and “system NPS”.<sup>10, 12</sup> There is a complete absence of a low-frequency drop in either the MTF or the NPS. This is due to the almost complete elimination of scattered radiation. This differs from area systems, where scatter can account for up to half of the x-ray flux incident on the detector in the absence of a grid. This benefit will also be present in the DQE (not presented here), as the scatter elimination is achieved without attenuating the primary radiation.

### 3.2. Clinical Trial

A clinical study of 30 patients is ongoing; to date, 9 women have been recruited and all have had clinical findings. Our initial goal was to seek anecdotal proof that the system provided clinically acceptable breast images. Criteria include breast positioning, resolution of high-contrast structures such as calcifications and clips, and resolution of larger low-contrast objects such as masses and cysts. A preliminary analysis indicates that the image quality achieved to date is acceptable. Figure 6 demonstrates the system being used for a medial-lateral oblique (MLO) mammogram. Breast positioning for both MLO and cranio-caudal (CC) mammograms appear to be acceptable; examples of both are provided in Figure 6. The MLO image, reconstructed near the mid-plane of the breast, shows that the pectoralis muscle extends below the line drawn perpendicular to the muscle that passes through the nipple (shown with the arrow). The CC image clearly shows the posterior margin of the glandular tissue.

The images to date have shown very high spatial resolution. In general, we see more calcifications in the tomosynthesis images than in the screen-film mammograms. Further, the calcifications in the tomosynthesis images are generally better resolved (sharper and having higher contrast) than in the screen-film images. We find that calcifications rapidly disappear when out-of-plane. These observations are consistent with our previous findings with phantoms and animals, and are likely due to the choice of angular range, number of projection images and pixel size.<sup>7</sup>

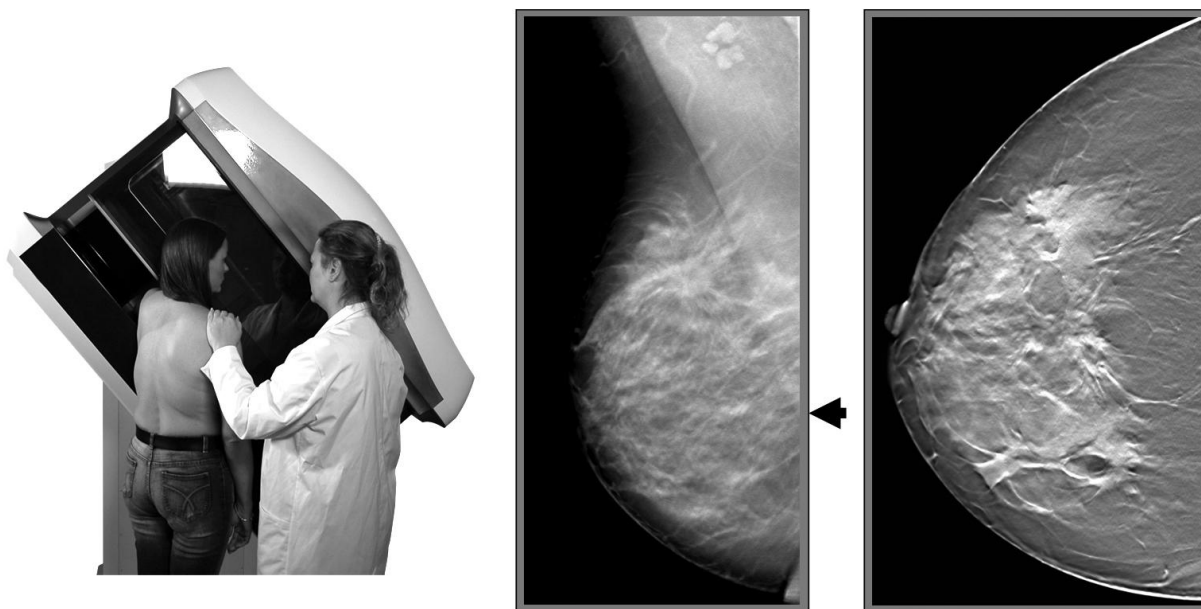


**Figure 6:** The imaging system is shown (left) with a model, demonstrating the positioning used for a MLO tomosynthesis image. A MLO image is shown in the center. The pectoralis muscle extends to below the perpendicular line from the muscle to the nipple (arrow). A CC image is shown on the right. This image shows the posterior margin of the glandular tissue. These two images clearly demonstrate that good clinical breast positioning is possible with the system.

Large low-contrast objects have also been well visualized. The images (see Figures 6-8) depict the breast anatomy well. The glandular tissue, adipose tissue, Cooper's ligaments, blood vessels, lymph nodes and other structures of the breast are well depicted. To date, we have found one cancer (Figure 7), which was quite obvious in the tomosynthesis image, and only marginally visible in the screen-film image. While anecdotal, we believe that these early images provide convincing evidence of the superiority of both tomosynthesis and our approach of simultaneously acquiring multiple images with a scanning photon-counting detector. We believe that the system is capable of clinical quality images, with adequate tissue penetration and breast positioning. Admittedly, these results are preliminary and lack statistical significance.

These initial images have been acquired at an AGD that is comparable to the screen-film examination of a 4 cm thick breast. The technique for the screen-film mammograms ranged from 30 to 31 kVp and from 21 to 166 mAs, resulting in an entrance skin air kerma (ESAK) of between 2.91 and 21.75 mGy (mean value of 7.31 mGy) and an AGD of between 0.91 and 3.50 mGy (mean value of 1.56 mGy). The digital tomosynthesis images were acquired with a technique 35 kVp, 140 to 180 mAs. This resulted in an ESAK of between 4.33 and 5.61 mGy (mean value of 4.83 mGy) and an AGD of between 1.11 and 1.67 mGy (mean value of 1.45 mGy). It should be noted that the first 6 patients were imaged with 40 active linear detectors, while the last 3 patients were imaged with the full set of 48 linear detectors; as such, the AGD for the first 6 patients (1.42 mGy) is lower than for the last 3 patients (1.50 mGy).

As with any study comparing dose, it is important to realize that the dose in a digital image is somewhat arbitrary, as the system is linear and has very wide dynamic range. The relevant questions are: (1) is the resultant image x-ray quantum noise limited to high spatial-frequency; and (2) are the images of clinical quality. We believe that the data presented in Section 3.1 are proof of the former. We further believe that the results in this section provide anecdotal proof of the latter, for it is notable that the tomosynthesis images were acquired at a lower dose than the screen-film mammograms, yet appear to have comparable or superior image quality.

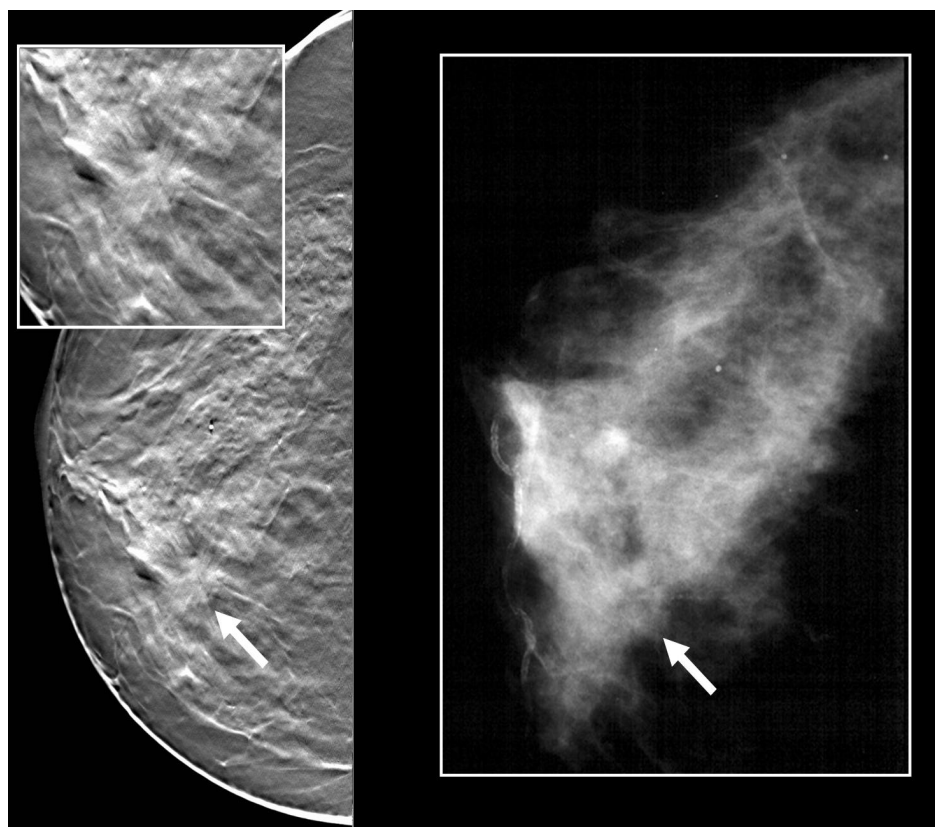


**Figure 7:** A tomographic image (left), and screen-film image (right) are shown. The location of a ductal carcinoma is indicated by the arrows. The tomographic plane was chosen so that the tumor was in focus. The screen-film image was windowed and leveled after digitization to best demonstrate the tumor; however, the tumor is not well-visualized. In the tomosynthesis image, the tumor is well depicted. A magnified view is also provided.

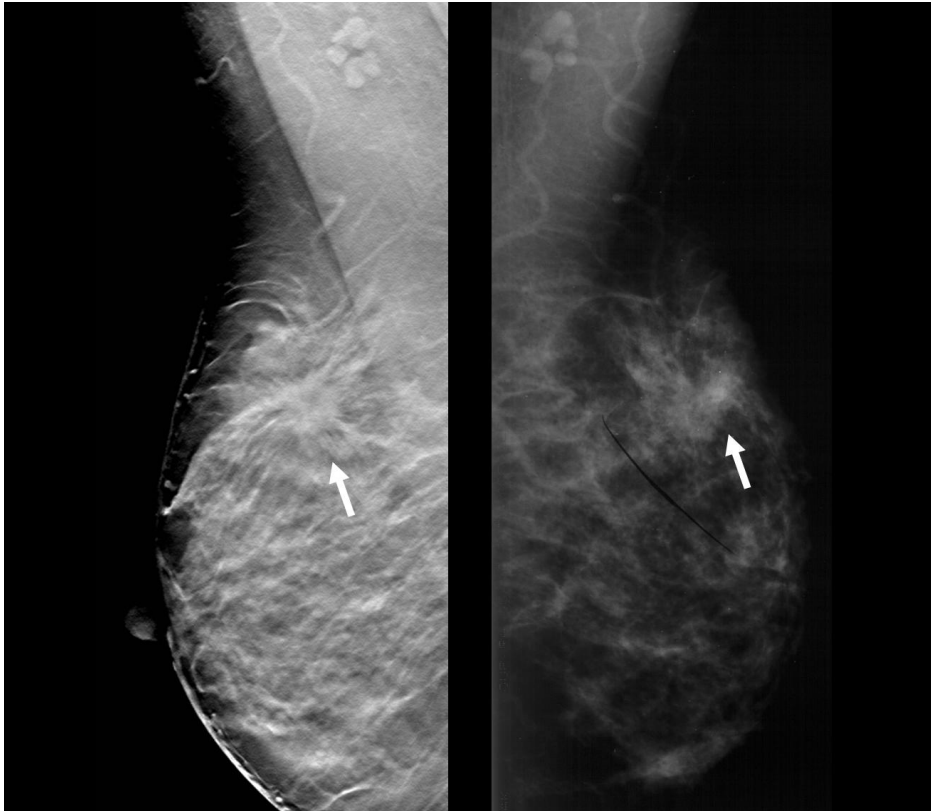


**Figure 8:** A tomographic image (left), and screen-film image (right) are shown. The location of a ductal carcinoma is indicated by the arrows. The tomographic plane was chosen so that the tumor was in focus. The tumor is much better visualized in the tomographic image. The extent of the tumor is also better portrayed.

### 3.3. Simulation of the Number of Projections on Image Quality

Continuing our work from last year,<sup>7</sup> we have again examined the effect of the number of projections on image quality. Consider the tomographic image of a tumor shown in Figure 9. The images were reconstructed with (a) 48 projection angles, (b) 24 projection angles, and (d) 12 projection angles, by uniformly sampling from the full set of 48 projection images. The images were all reconstructed over the same range of projection angles. The reconstructed images were then processed so as to have comparable quantum noise. Thus, the differences in the image arise primarily due to differences in the number of projection images used.

The difference between images (a) and (b) is shown in image (c). The difference images have been offset so that the average value is in the middle of the grayscale range. Here, the main differences occur on the periphery of the breast, and along other structures with edges. The difference between images (a) and (d) is shown in image (e). In (e) there are significant differences seen throughout the breast, including structures within the tumor. These structures again appear to relate mostly to edge information, but do appear to include some grayscale (i.e., lower spatial frequency) information.

Again, it should be noted that these results are anecdotal. However, after examining many such images, we believe that it is essential that tomographic images of the breast be acquired with as many unique projection angles as possible. We further believe that these clinical examples support our prior research.<sup>7</sup> A more complete reader study will be necessary to test whether these differences result in statistically significant differences in clinical performance.

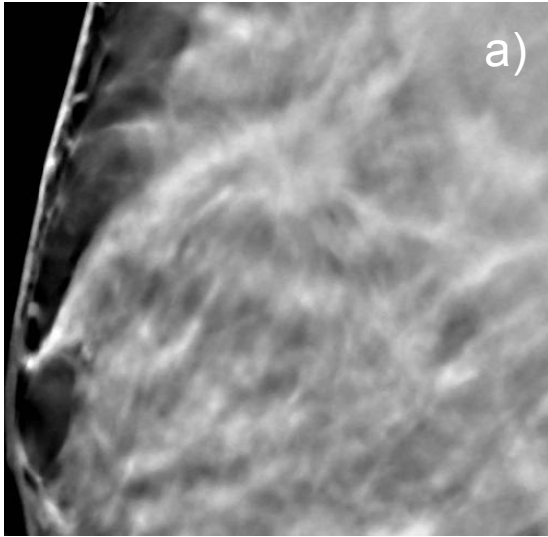
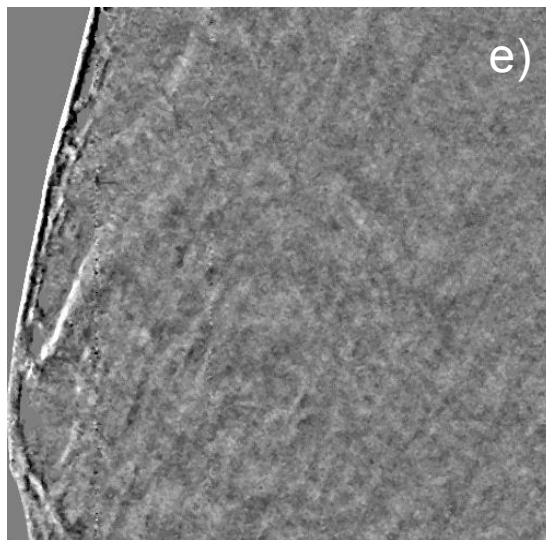
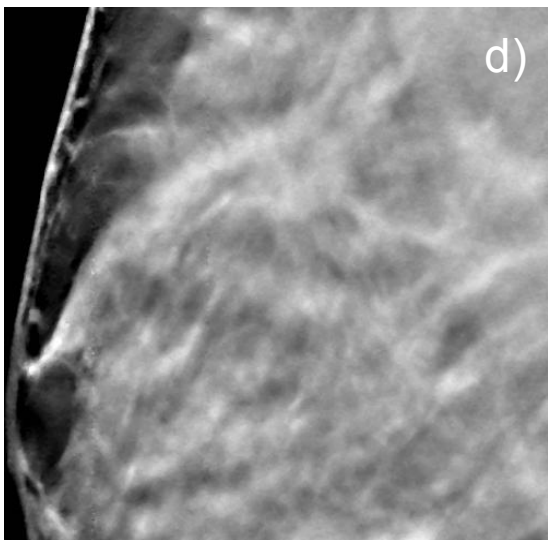
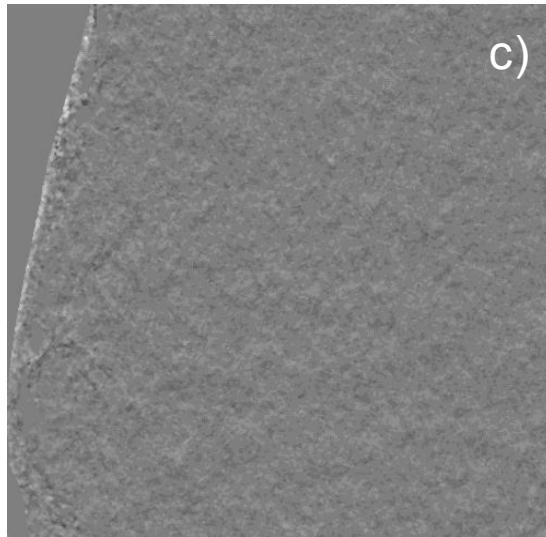
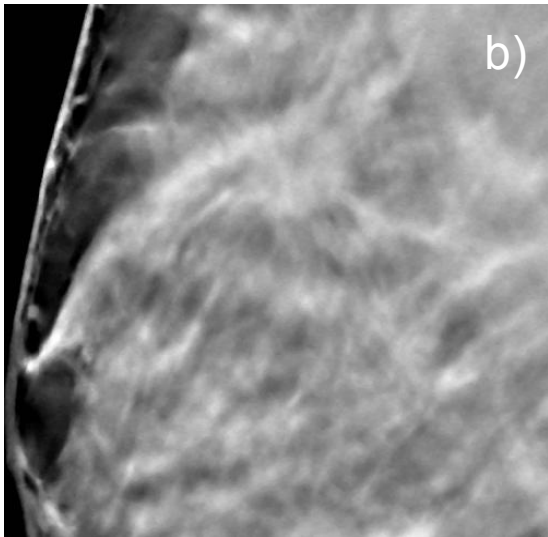


**Figure 9:** Tomographic images of a tumor are shown. These images were reconstructed with (a) 48 projection angles, (b) 24 projection angles, and (d) 12 projection angles. The images were reconstructed over the same range of projection angles. The images were processed so as to have comparable quantum noise. The difference between (a) and (b) is shown in (c). The difference images have been offset so that the average value is in the middle of the grayscale range. In (c), the main differences occur on the periphery of the breast, and along other edges. The difference between (a) and (d) is shown in (e). In (e) there are significant differences seen throughout the breast, including structures within the tumor.



## 4. CONCLUSION

A clinical photon-counting tomosynthesis imaging system has been developed and is in clinical trials. A preliminary assessment of tomosynthesis image quality has been performed with both qualitative and quantitative methods. The measured values of MTF and NPS appear concordant with theoretical values. The MTF in the scanning direction is dominated by scanning unsharpness and geometric factors. The NPS in the same direction demonstrates that the acquired data are uncorrelated between acquisition lines (i.e., separated in time). This would indicate that the system is free of lag. The MTF and NPS in the strip direction are somewhat lower than in the scan direction; this is believed to be related to simultaneous triggering of adjacent channels in the detector array. The reconstructed NPS show a slight decrease with increasing spatial frequency. We believe that this is related to the sampling and interpolation of rays in the reconstruction process.

A phase I clinical trial is ongoing. To date, 9 of 30 women have been recruited. The clinical image quality has been assessed qualitatively. Breast positioning appears to be similar to other digital and screen-film imaging systems. The visualization of breast anatomy (both normal and malignant) appears to be comparable or superior to screen-film mammography, at an AGD comparable to screen-film mammography. Examination of images reconstructed with a sub-sampled set of tomographic images appears to support the hypothesis that image quality is superior when more projection images are used in the reconstruction. These results are anecdotal; a larger reader trial is necessary to demonstrate whether these results are clinically significant.

## ACKNOWLEDGEMENTS

The authors would like to acknowledge the assistance of Dr. Per Sunden of Danderyds Sjukhus AB (Stockholm) for his assistance in the clinical trial. This work is partially funded by NIH grant PO1 CA85484.

## REFERENCES

1. L. Ma, E. Fishell, B. Wright, W. Hanna, S. Allan, and N. F. Boyd, "Case-control study of factors associated with failure to detect breast cancer by mammography.," *Journal of the National Cancer Institute* **84**(10), 781-785 (1992).
2. L. T. Niklason, B. T. Christian, L. E. Niklason, D. B. Kopans, D. E. Castleberry, B. H. Opsahl-Ong, C. E. Landberg, P. J. Slanetz, A. A. Giardino, R. Moore, D. Albagli, M. C. DeJule, P. F. Fitzgerald, D. F. Fobare, B. W. Giambattista, R. F. Kwasnick, J. Liu, S. J. Lubowski, G. E. Possin, J. F. Richotte, C. Y. Wei, and R. F. Wirth, "Digital tomosynthesis in breast imaging," *Radiology* **205**(2), 399-406 (1997).
3. J. T. Dobbins, 3rd and D. J. Godfrey, "Digital x-ray tomosynthesis: current state of the art and clinical potential," *Physics in Medicine & Biology* **48**(19), R65-106 (2003).
4. S. Thunberg and e. al, "Evaluation of a Photon Counting Mammography System," presented at the SPIE Medical Imaging 2002, **4682**, 202-208 (2002).
5. S. Thunberg, A. D. A. Maidment, and e. al., "Dose reduction in Mammography with Photon Counting Imaging," presented at the SPIE Medical Imaging 2004, **5368**, 457-465 (2004).
6. S. Thunberg, A. D. A. Maidment, and e. al., "Tomosynthesis with a Multi-line Photon Counting Camera," presented at the 7th International Workshop on Digital Mammography, 459-465 (2004).
7. A. D. A. Maidment, M. Albert, S. Thunberg, L. AdelÖw, O. Blom, J. EgerstrÖm, M. Eklund, T. Francke, U. Jordung, T. Kristoffersson, K. Lindman, L. Lindqvist, D. Marchal, H. Olla, E. Penton, J. Rantanen, S. Solokov, C. Ullberg, and N. Weber, "Evaluation of a Photon-Counting Breast Tomosynthesis Imaging System," presented at the SPIE Medical Imaging 2005, **5745**, 572-582 (2005).
8. J. H. Siewerdsen and D. A. Jaffray, "A ghost story: spatio-temporal response characteristics of an indirect-detection flat-panel imager," *Medical Physics* **26**(8), 1624-1641 (1999).
9. Y.-H. Kao, A. D. A. Maidment, M. Albert, A.-K. Carton, and H. Bosmans, "Assessment of a software tool for measurement of the modulation transfer function," presented at the Medical Imaging 2005: Physics of Medical Imaging, **5745**, 1199-1208 (2005).
10. A. K. Carton, D. Vandenbroucke, L. Struye, A. D. Maidment, Y. H. Kao, M. Albert, H. Bosmans, and G. Marchal, "Validation of MTF measurement for digital mammography quality control," *Medical Physics* **32**(6), 1684-1695 (2005).

11. A. D. A. Maidment and M. Albert, "Conditioning data for calculation of the modulation transfer function," *Medical Physics* **30**(2), 248-253 (2003).
12. Z. Shen, G. Mawdsley, A. Bloomquist, J. Mainprize, and M. Yaffe, "Interpreting system MTF and NPS measured on clinical digital mammography systems," presented at the Digital Mammography IWDM 2002, 123-127 (2002).
13. J. S. Bendat and A. G. Piersol, *Random Data: Analysis and Measurement Procedures*, 2nd Edition ed. (Wiley-Interscience, New York, 1986).